Predictive Torque Control for Inverter-Fed Induction Machines

Pablo Correa, *Student Member, IEEE*, Mario Pacas, *Senior Member, IEEE*, and José Rodríguez, *Senior Member, IEEE*

***Abstract*—This paper presents a predictive control scheme that is suitable for the torque and flux control of multilevel inverter-fed induction machines. The control strategy combines the use of a proportional–integral controller to obtain good steady-state behavior and a predictive controller to achieve fast dynamic torque response. In this way, torque and stator flux references can be reached within one sample period. With the use of multilevel space phasor modulation, low torque and flux ripple are possible with fixed sample rate. Experimental and simulation results are presented in order to demonstrate the effectiveness of the proposed strategy.**

***Index Terms*—Induction motor drives, predictive control, variable-speed drives.**

NOMENCLATURE

$\underline{u}_1$, $\underline{i}_1$, $\underline{\psi}_1$	Stator voltage, current, and flux space phasors.
$\underline{i}_2$, $\underline{\psi}_2$	Rotor current and rotor flux space phasors.
R_1, L_1	Stator winding resistance and stator self-inductance.
R_2, L_2	Rotor winding resistance and rotor self-inductance.
L_h	Magnetizing inductance.
M, M_L	Electromagnetic torque and load torque.
Ω, γ	Mechanical rotor speed and electrical rotor angle.
J, p	Total inertia and the number of pole pairs.

I. INTRODUCTION

MANY industrial processes require high torque dynamics and low torque ripple to obtain a high-quality product. In commercial drives, two widely used control schemes achieve high torque dynamics: field-oriented control and direct torque control (DTC). The main difference between both control strategies lies in the fact that DTC is a "bang-bang" control characterized by the absence of proportional–integral (PI) controllers in the torque and flux control loops, and it does not use a modulator to synthesize the output voltage. The dynamic of this control method is excellent, but their implementation requires a short sampling time ($\mathrm{Ts} < 25\ \mu\mathrm{s}$) and presents some drawbacks such as variable switching frequency in the power semiconductors [1]. For these reasons, a DTC strategy cannot directly be compared with modulator-based strategies working with larger sampling times and at a constant switching frequency. New control schemes have been investigated in the last years, aiming the improvement of the dynamics of the torque response [2], [3], which is mainly focused on predictive control methods [4]. In this category falls predictive direct mean torque control (DMTC) [5], field-oriented control using dead-beat principles [6], or concepts of generalized predictive control [7].

The development of high-performance control strategies in multilevel inverters has been mainly oriented to strategies such as DTC [8], direct self control (DSC) [9], and predictive control based on DMTC [10], [11]. On the other hand, methods based on a modulator such as field-oriented control can be directly applied in multilevel inverters, and they are integrated in several commercial drives [12].

In this paper, the idea of a one-step predictive control is used, based on the assumption of an accurate model of the machine. The proposed method uses a PI controller to improve the optimal steady-state behavior in combination with a predictive dead-beat controller to achieve fast torque response. In this way, torque and stator flux references can be reached within one sampling period if enough voltage reserve is available. The strategy is applied in an H-bridge multilevel inverter topology with space phasor modulation (SPM) to obtain low torque ripple. Experimental results in a three-level and a five-level H-bridge inverter are presented in this paper to evaluate the feasibility of the proposed method.

II. INVERTER TOPOLOGY

Multilevel inverter topologies were introduced initially as a mean to reduce the harmonic content of the output waveform, as was described in an early work in 1981 [13]. In contrast with the two-level inverter, the multilevel topology has the ability to synthesize an output-voltage waveform with three or more levels, obtaining currents with reduced harmonic distortion and a smaller torque ripple in the shaft. Furthermore, the resulting output voltage could be increased beyond the voltage rating of the individual power devices, making the topology particularly attractive for medium-voltage applications.

The cascaded H-bridge voltage source inverter topology depicted in Fig. 1 was considered in this paper [14]. Each cell is composed of a diode rectifier, a dc-link capacitor, and a single-phase H-bridge inverter. It can be easily verified that an

Manuscript received November 17, 2005; revised July 4, 2006. Abstract published on the Internet January 14, 2007. This work was supported in part by the German Service for Academic Interchange (DAAD) and in part by the Dirección de Investigación of the Universidad Técnica Federico Santa María. This paper was presented at the IEEE Power Electronics Specialists Conference, Recife, Brazil, June 11–16, 2005.

P. Correa and M. Pacas are with Siegen University, 57068 Siegen, Germany (e-mail: p.correavasquez@uni-siegen.de; jmpacas@ieee.org).

J. Rodríguez is with the Universidad Técnica Federico Santa María, Valparaíso 2390240, Chile (e-mail: jrp@elo.utfsm.cl).

Digital Object Identifier 10.1109/TIE.2007.892628

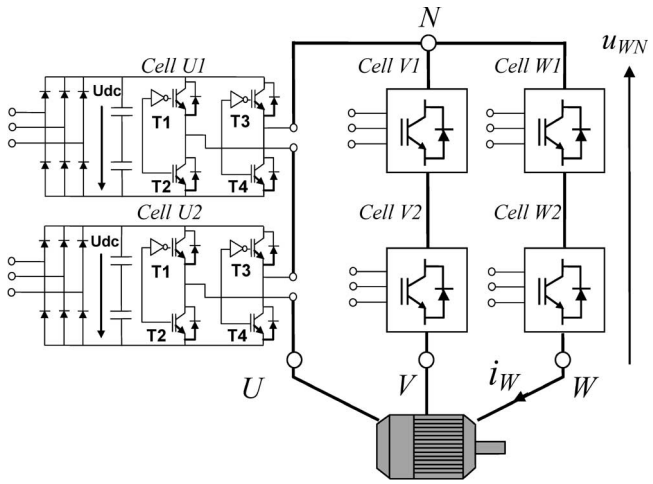

Fig. 1. Simplified scheme of a five-level cascaded multilevel inverter topology.

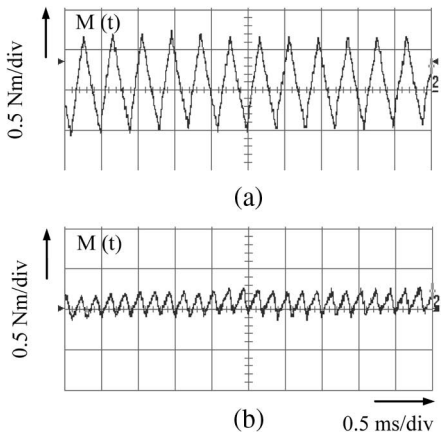

Fig. 2. Torque ripple at no-load condition generated by a multilevel inverter with SPM, $U_{\rm dc} = 120$ V, $\Psi_1^* = 0.42$ Vs, $\Omega = 314$ min^{-1}, and switching frequency $f_s = 1.25$ kHz. (a) Three-level inverter. (b) Five-level inverter.

inverter with one cell synthesizes stepped waveforms with three voltage levels $U_{\rm dc}$, 0, $-U_{\rm dc}$, and each extra cell adds two extra levels per phase. The addition of extra cells permits to locate also the first band of high-order harmonics at higher frequencies, resulting in a twofold reduction effect in the torque ripple. Fig. 2 shows a comparison between the torque ripple obtained with a three-level inverter and a five-level inverter working with the same switching frequency at no load ($M^* = 0$, $n = 314$ min^{-1}). The torque ripple is reduced to approximately 25% compared to the three-level inverter.

III. Mathematical Model

For the modeling of the induction machine, the following assumptions were made.

- The neutral point is not connected.
- There are no eddy currents or core losses in the stator and rotor.
- Only the fundamental wave of the air-gap field is considered for the calculation of the inductances.

Using these assumptions, which are common to the modeling of electrical machines, the induction machine will be described by the following well-known set of complex equations in the stator reference frame:

$$\underline{u}_1 = \underline{i}_1 \cdot R_1 + \frac{d}{dt}\underline{\psi}_1 \tag{1}$$

$$0 = \underline{i}'_2 \cdot R'_2 - j \cdot \dot{\gamma} \cdot \underline{\psi}'_2 + \frac{d}{dt}\underline{\psi}'_2. \tag{2}$$

The fluxes and currents are related by

$$\underline{\psi}_1 = L_1 \cdot \underline{\mathrm{i}}_1 + L_h \cdot \underline{i}'_2 \tag{3}$$

$$\underline{\psi}'_2 = L_h \cdot \underline{\mathrm{i}}_1 + L'_2 \cdot \underline{\mathrm{i}}'_2 \tag{4}$$

and the electromagnetic torque is given by

$$M = \frac{3}{2} \cdot p \cdot \frac{L_h}{\sigma \cdot L_1 \cdot L'_2} |\underline{\psi}_1| |\underline{\psi}'_2| \sin(\vartheta_{12}). \tag{5}$$

With the mechanical equation

$$M - M_L = J\frac{d\Omega}{dt} = \frac{J}{p} \cdot \frac{d\dot{\gamma}}{dt} \tag{6}$$

the machine model is fully described.

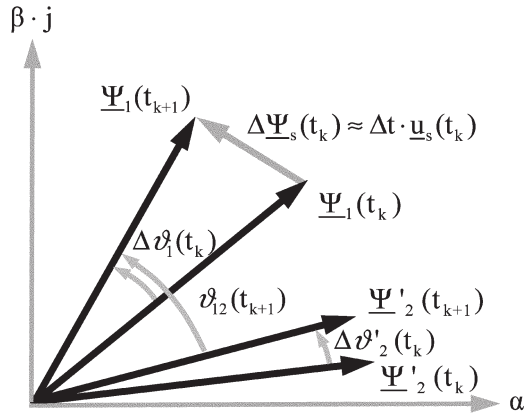

Fig. 3. Stator and rotor flux space phasors for $t = t_k$ and $t = t_{k+1}$.

IV. Control Strategy

A. Basic Operation Principle

The presented control method, such as all DTC methods, is based on the control of the magnitude and phase of the stator flux space phasor through the proper choice of the stator voltage space phasor. From (1) and under the assumption of constant magnitude of stator and rotor fluxes, it is clear that a fast torque change can be achieved with a change of angle ϑ_{12} between both fluxes. Since the sample time of the controller is smaller than the rotor time constant, the variation in the trajectory of the rotor flux during the sample time interval can be neglected. Hence, the stator flux space phasor is the main quantity influencing torque development.

An example of the control principle is shown in Fig. 3. If an increase of the torque is needed, the angle variation of the stator flux $\Delta\vartheta_1$ must be larger than the angle variation of the rotor flux $\Delta\vartheta_2$ in a sample time, and vice versa.

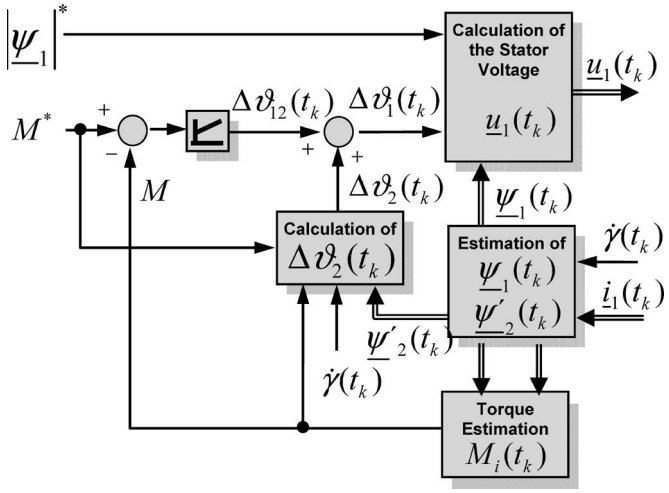

Fig. 4. Simplified structure of the control scheme.

The stator-flux space phasor in the next sample time, corresponding to the desired torque value, is determined by

$$\underline{\psi}_1(t_{k+1}) = \left|\underline{\psi}_1^*(t_{k+1})\right| \cdot e^{j(\Delta\vartheta_1(t_k)+\vartheta_1(t_k))} \tag{7}$$

with $\Delta\vartheta_1(t_k)$ defined as

$$\Delta\vartheta_1(t_k) = \Delta\vartheta_{12}(t_k) + \Delta\vartheta_2(t_k). \tag{8}$$

Finally, the appropriate stator-voltage phasor $\underline{u}_1$ can be found using (1) after discretization, i.e.,

$$\underline{u}_1(t_k) = \frac{\underline{\psi}_1(t_{k+1}) - \underline{\psi}_1(t_k)}{T_s} + R_1 \cdot \underline{i}_1(t_k). \tag{9}$$

With (9), the calculated voltage space phasor can be synthesized using SPM.

Fig. 4 shows the basic structure of the controller. The torque reference is subtracted from an estimated value calculated with the phase currents and electrical rotor angle. This difference is supplied to a PI controller, which delivers the variation of the angle $\Delta\vartheta_{12}$. The task of the integral part of the controller is supported by the addition of the term $\Delta\vartheta_2(t_k)$ as a feedforward [15], i.e.,

$$\Delta\vartheta_2(t_k) = \left(\dot{\gamma} + \frac{2R_2' \cdot M_i^*}{3p\left|\underline{\psi}_2(t_k)\right|^2}\right) T_s. \tag{10}$$

Although a PI controller has advantages, e.g., zero steady-state error and robustness, this controller has only a moderate dynamic performance in comparison with a dead-beat strategy. In order to improve the dynamic behavior, the difference $\Delta\vartheta_{12}(t_{k+1})$ can be predicted to reach the torque reference in the quickest way possible.

B. Dead-Beat Operation

Dead-beat control aims the best possible dynamic response of a system. That means that, after a time period equal to the sample period, the controlled variables should reach the set point and remain there [16]. In order to obtain a dead-beat system response, (5) can be used to calculate the slip angle $\vartheta_{12}(t_{k+1})$, which fulfills the requirement of torque in the next sample time as follows:

$$\vartheta_{12}(t_{k+1}) = \arcsin\left(\frac{2}{3} \cdot \frac{M^*(t_{k+1}) \cdot \sigma \cdot L_1 \cdot L_2'}{p \cdot L_h \cdot \psi_1^*(t_{k+1}) \cdot \psi_2'(t_k)}\right). \tag{11}$$

Thus, the output for the dead-beat control is determined by

$$\Delta\vartheta_{12}(t_k) = \vartheta_{12}(t_{k+1}) - \vartheta_{12}(t_k). \tag{12}$$

By assuming a perfect model of the inverter-motor system, the torque reference should be reached in the next sample time. However, for large changes of the desired torque, especially in the range of high rotor speeds, the stator voltage calculated by (9) could have a magnitude beyond the maximum output voltage of the inverter. In this case, the controller operates with the maximum voltage possible to obtain a torque in the next sample time that is as close as possible to the reference. As soon as the torque reaches the tolerance band of width ε around the torque reference, i.e.,

$$-\varepsilon \le M - M^* \le \varepsilon \tag{13}$$

the operation of the PI controller can be resumed. A soft transition between both operating modes can be achieved if the integral part of the PI controller is preloaded with a predicted angle variation for the next sample time.

It should be noted that the equations were expressed with only one step in the future, assuming that the time for calculations can be neglected. Considering that the calculation of the control algorithm needs some time, the value predicted in the real algorithm corresponds actually to t_{k+2}. Thus, the output voltage is calculated for the next sample time t_{k+1}, and the reference values of torque and flux are reached in t_{k+2}. A diagram of the control strategy is presented in Fig. 5.

C. Multilevel Modulator

Commercial versions of the H-bridge multilevel inverter use the phase-shift multilevel pulse width modulation (PWM) method to generate an output waveform with multiple levels [17]. This modulation strategy is easy to implement and operates the power switches with constant switching frequency, but it has higher harmonic content in comparison to other strategies such as phase-disposition PWM and SPM [18]. In this paper, SPM will be considered to synthesize the output voltages.

The high number of freedom degrees of multilevel H-Bridge inverters makes the implementation of SPM more complicated than the standard two-level case. Taking as example the five-level multicell inverter presented in Fig. 1, there are 125 output-voltage combinations available, which generate the 61 different inverter voltage space phasors depicted by dots in Fig. 6(a). The problem of identifying the optimum set of inverter space phasors for a given reference was solved in [19], where a linear coordinate transformation is used to simplify the search algorithm, and it is demonstrated that the harmonic content of the output-voltage waveform is minimized when the three

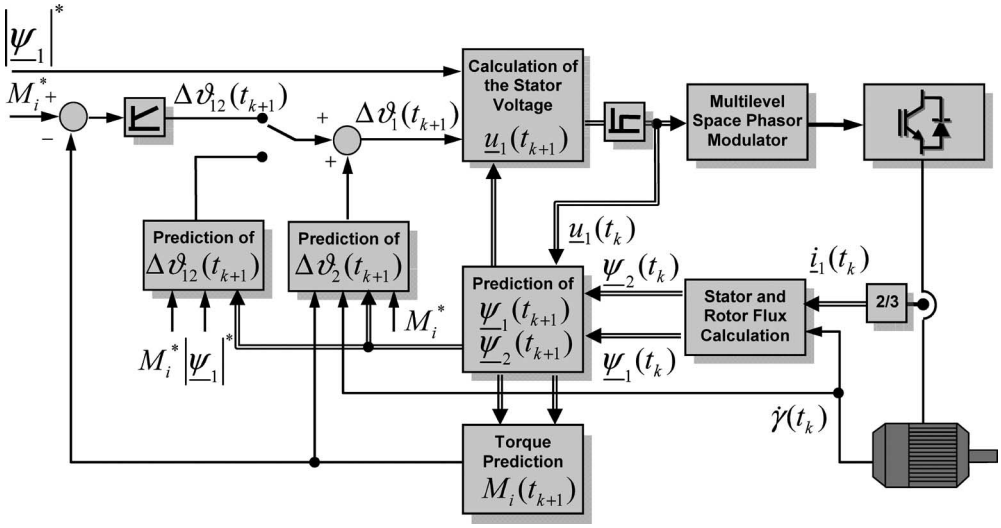

Fig. 5. Scheme of the predictive torque control.

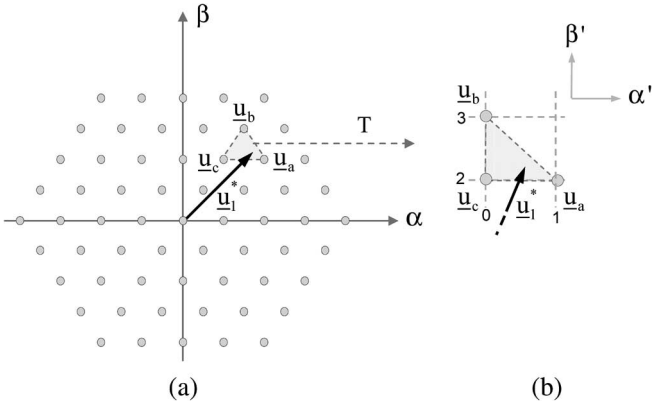

Fig. 6. (a) Inverter space voltage phasors for a five-level inverter. (b) Effect of the transformation on the selected sector.

nearest space voltage phasors are used. The selection of the three nearest space phasors can be simplified by using transformations, which locate the reference space phasor voltage $\underline{u}_1^*$ in a new coordinate system, where the position of each inverter voltage space phasor is described only by integer numbers [Fig. 6(b)], i.e.,

$$\underline{u}_1'(t_k)^* = \begin{bmatrix} 3/2 & -\sqrt{3}/2 \\ 0 & \sqrt{3} \end{bmatrix} \underline{u}_1(t_k)^*. \tag{14}$$

In this way, the coordinates for the three nearest inverter space voltage phasors $\underline{u}_a$, $\underline{u}_b$, and $\underline{u}_c$ are determined by applying the smallest elementary-approximation-function integer greater than x, i.e., ceil(x), and the greatest integer smaller than or equal to x, i.e., floor(x), to the real and imaginary parts of $\underline{u}_1^*$ as follows:

$$\left.\begin{array}{l} \underline{u}_a' = \text{ceil Re}(\underline{u}^{*\prime}) + \text{floor Im}(\underline{u}^{*\prime})j \\ \underline{u}_b' = \text{floor Re}(\underline{u}^{*\prime}) + \text{ceil Im}(\underline{u}^{*\prime})j \\ \text{if} \quad ((\text{Re}(\underline{u}^{*\prime}) + \text{Im}(\underline{u}^{*\prime})) - (\text{Re}(\underline{u}_1') + \text{Im}(\underline{u}_1'))) > 0 \\ \qquad \underline{u}_c' = \text{ceil Re}(\underline{u}^{*\prime}) + \text{ceil Im}(\underline{u}^{*\prime})j \\ \text{else} \\ \qquad \underline{u}_c' = \text{floor Re}(\underline{u}^{*\prime}) + \text{floor Im}(\underline{u}^{*\prime})j \end{array}\right\}. \tag{15}$$

Once the three voltage space phasors are determined, the duty cycles can be calculated using the projections of the space phasors on the side of the respective sector. The projections in this case are given by the fractional parts of the reference space phasor $\underline{u}^{*\prime}$

$$\left.\begin{array}{l} d_a = |\text{Re}(\underline{u}_c' - \underline{u}^{*\prime})| \\ d_b = |\text{Im}(\underline{u}_c' - \underline{u}^{*\prime})| \\ d_c = 1 - d_a - d_b \end{array}\right\}. \tag{16}$$

The next step in the modulation algorithm is to determine the optimal sequence for the selected space phasors, in order to minimize the number of switching transitions. This analysis was made in [18], taking into account all the three-phase output-voltage combinations associated to each space phasor of the selected sector. A different approach is proposed in this paper, based on a 3-D representation of the space voltage phasors. Including common-mode voltage u_{cm} as an extra axis perpendicular to the $\alpha-\beta$ plane, each three-phase output voltage will be defined by only one vector. The minimum number of switching transitions in each phase is obtained by choosing a sequence of vectors arranged with an increasing or decreasing common-mode voltage (Fig. 7).

An extra optimization degree can be obtained if the selected three-phase voltage set has minimum common-mode voltage. Finally, the firing pulses are distributed evenly through the cells by using the state machine suggested in [20], reducing in this way the switching frequency of the power semiconductors. As shown in Fig. 8(a) for a modulator operating with a period of 200 μs and modulation index $m = 0.7$, the line-to-line voltage has higher harmonic content at the fundamental frequency f_1 and the first high-order harmonic band centered at the modulation frequency $f_o = 5$ kHz. On the other hand, the firing pulses delivered to the power semiconductors have lower switching frequency, with the first high-order harmonic band located at a quarter of the modulation frequency; in this case, $f_s = 1.25$ kHz [Fig. 8(b)].

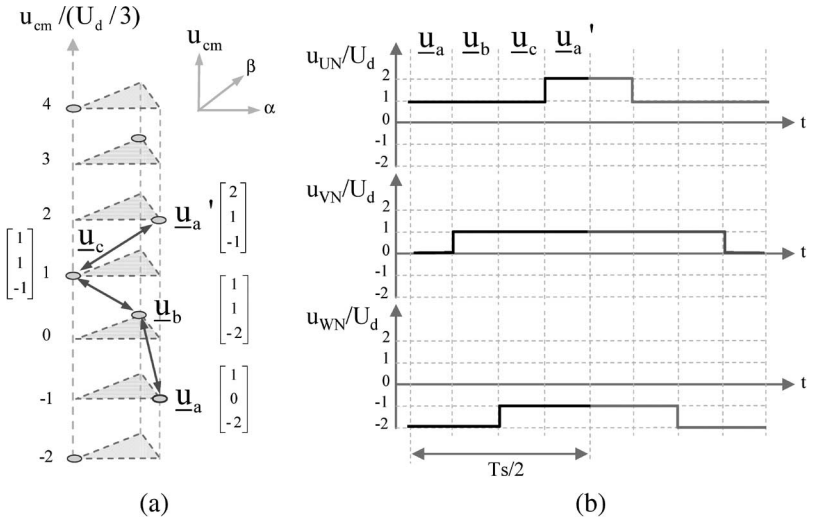

Fig. 7. (a) Three-phase output voltages and their locations in the space voltage phasor diagram including the common-mode voltage. (b) Resulting phase output voltages for the respective sequence.

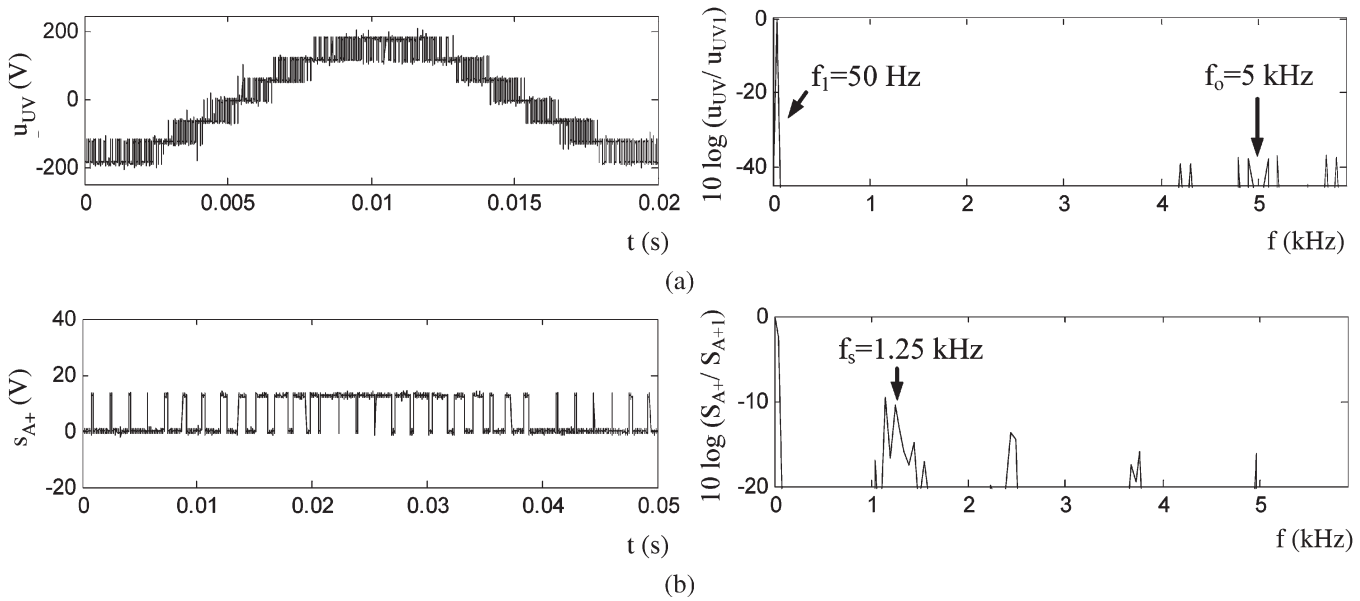

Fig. 8. (a) Line-to-line voltage waveform with SPM and the corresponding frequency spectrum. (b) Firing pulses in one transistor and the corresponding frequency spectrum (experimental result with $U_{\rm dc} = 65$ V).

V. Experimental Setup

A 15-kW prototype of a multicell inverter was developed in order to verify the proposed control method. Each cell is composed of a three-phase rectifier, a dc link of up to 250 V, and four insulated gate bipolar transistors (IGBTs) IRG4PH40UD of 21-A nominal current with their respective drivers (Fig. 9). A floating-point digital-signal-processor platform ADSP-21062 was used for the implementation of digital control. The modulator, the timers, and the incremental encoder were programmed in a field-programmable gate array included in the board. The sampling period was set up in 200 μs, defining a modulation frequency of 5 kHz. The multicell inverter was used to feed a 5.5-kW induction machine for the first tests. Fig. 10 presents the dynamic performance of the control algorithm at no-load conditions. A reference torque step equal to 9.1% of the rated value ($M_N = 35$ N $\cdot$ m) was applied with a dc-link voltage of 120 V and with the machine running an initial speed of 314 min^{-1}. Fig. 11 shows a zoom of the same transition, and as it can be seen, the calculated torque has a short rise time, and the magnitude of the stator flux remains unaffected (Fig. 11). The dynamic behavior of the dead-beat controller depends strongly on the capacity of the converter to deliver enough voltage. If the step in the torque reference is large enough, especially in the high-speed range, the controller calculates a reference voltage $\underline{u}_1^*$ with a modulation index greater than the maximum. In this case, a stator voltage phasor with maximum amplitude is utilized, and extra sampling periods are necessary to reach the reference

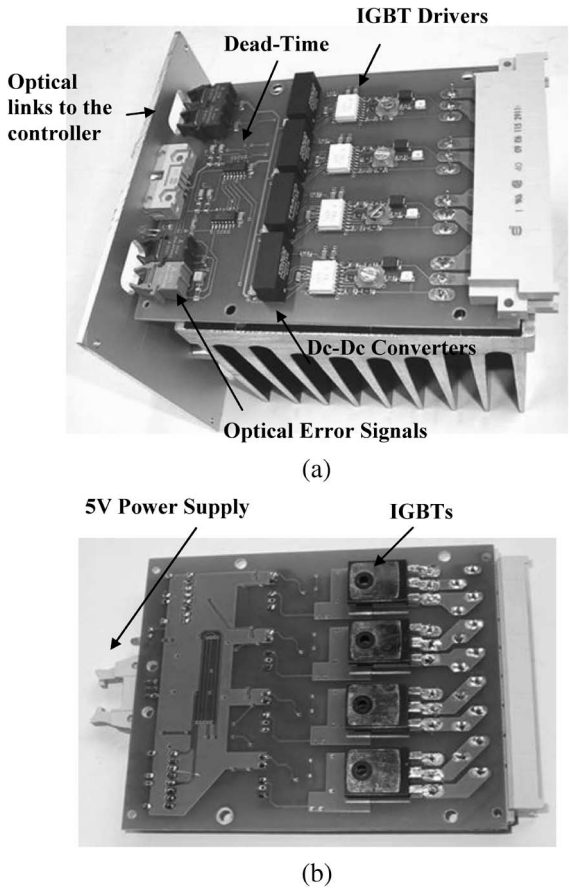

Fig. 9. Cell of the multilevel inverter. (a) Top side. (b) Bottom side.

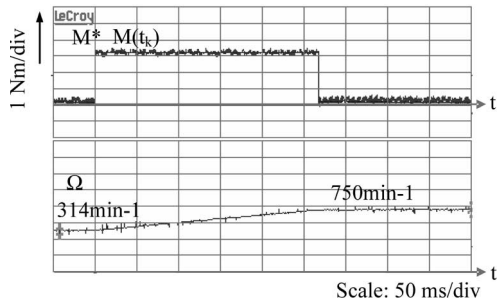

Fig. 10. Torque step of 0.091 M_N and rotor speed in a three-level inverter.

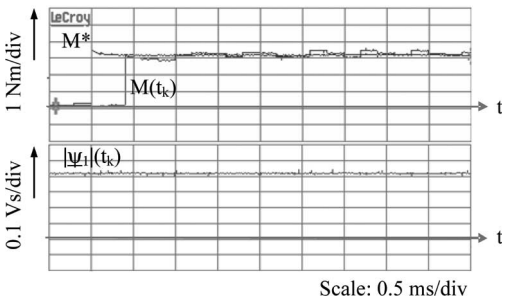

Fig. 11. Calculated torque for a step of 0.091 M_N and stator flux amplitude for a rotor speed of $\Omega = 314$ min^{-1} in a three-level inverter.

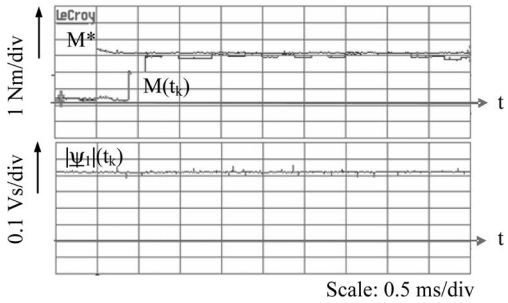

Fig. 12. Calculated torque for a step of 0.091 M_N and stator-flux amplitude for a rotor speed of $\Omega = 936$ min^{-1} in a three-level inverter.

value, as shown Fig. 12. In this case, the dynamic becomes comparable to a PI controller working in saturation. For this reason, the use of a dead-beat controller offers an advantage only in small-signal operation, as it is also the case in other predictive control strategies [21].

VI. Conclusion

An application of a high-performance control strategy for induction machines in multilevel inverters has been presented. The proposed control technique combines the use of a PI controller to obtain good steady-state behavior and a predictive controller to achieve very high dynamic in the torque. SPM with common-mode voltage reduction and minimization of the number of switching pulses is also proposed. Experimental results for a three-level and a five-level converter were obtained, showing low torque ripple and a high dynamic for small-signal torque changes.

References

[1] J.-K. Kang and S.-K. Sul, "New direct torque control of induction motor for minimum torque ripple and constant switching frequency," *IEEE Trans. Ind. Appl.*, vol. 35, no. 5, pp. 1076–1082, Sep./Oct. 1999.
[2] C. Lascu and A. M. Trzynadlowski, "A sensorless hybrid DTC drive for high-volume low-cost applications," *IEEE Trans. Ind. Electron.*, vol. 51, no. 5, pp. 1048–1055, Oct. 2004.
[3] ——, "Combining the principles of sliding mode, direct torque control, and space-vector modulation in a high-performance sensorless AC drive," *IEEE Trans. Ind. Appl.*, vol. 40, no. 1, pp. 170–177, Feb. 2006.
[4] R. Kennel and A. Linder, "Predictive control of inverter supplied electrical drives," in *Proc. IEEE PESC*, Galway, Ireland, Jun. 2000, CD-ROM.
[5] E. Flach, R. Hoffmann, and P. Mutschler, "Direct mean torque control of an induction motor," in *Proc. EPE*, Trondheim, Norway, 1997, vol. 3, pp. 672–677.
[6] D. Telford, M. W. Dunnigan, and B. W. Williams, "Adaptive high bandwidth current control for induction machines," *IEEE Trans. Power Electron.*, vol. 18, no. 2, pp. 527–538, Mar. 2003.
[7] R. Kennel, A. Linder, and M. Linke, "Generalized predictive control (GPC)—Ready for use in drive applications?" in *Proc. 32st IEEE PESC*, Vancouver, BC, Canada, 2001, vol. 4, pp.1839–1844.
[8] M. Escalante, J. C. Vannier, and A. Arzandé, "Flying capacitor multilevel inverters and DTC motor drive applications," *IEEE Trans. Ind. Electron.*, vol. 49, no. 4, pp. 809–815, Aug. 2002.
[9] M. Janssen and A. Steimel, "Direct self control with minimum torque ripple and high dynamics for a double three-level GTO inverter drive," *IEEE Trans. Ind. Electron.*, vol. 49, no. 5, pp. 1065–1071, Oct. 2002.
[10] C. Martins, X. Roboam, T. Meynard, and A. Carvalho, "Switching frequency imposition and ripple reduction in DTC drives by using multilevel converter," *IEEE Trans. Power Electron.*, vol. 17, no. 2, pp. 286–297, Mar. 2002.
[11] J. Rodríguez, J. Pontt, S. Kouro, and P. Correa, "Direct torque control with imposed switching frequency in an 11-level cascaded inverter," *IEEE Trans. Ind. Electron.*, vol. 51, no. 4, pp. 827–833, Aug. 2004.

[12] S. Bernet, "State of the art and developments of medium voltage converters—An overview," in *Proc. Int. Conf. PELINCEC*, Warsaw, Poland, Oct. 16–19, 2005, CD-ROM.
[13] A. Nabae, I. Takahashi, and H. Akagi, "A new neutral-point clamped PWM inverter," *IEEE Trans. Ind. Appl.*, vol. IA-17, no. 5, pp. 518–523, Sep./Oct. 1981.
[14] P. W. Hammond, "Medium voltage PWM drive and method," U.S. Patent 5 625 545, Apr. 29, 1997.
[15] M. Depenbrock and A. Steimel, "Speed-sensorless stator-flux-oriented control of induction motor drives in traction," in *Proc. IEEE IECON*, Roanoke, VA, Nov. 2–6, 2003, pp. 65–73.
[16] O. Föllinger, *Lineare Abtastsysteme*, 5th ed. Munich, Germany: Oldenbourg-Verlag, 1993.
[17] P. W. Hammond, "Drive and power supply with phase shifted carriers," U.S. Patent 6 411 530, Jun. 25, 2000.
[18] B. P. McGrath, D. G. Holmes, and T. A. Lipo, "Optimised space vector switching sequences for mutilevel inverters," in *Proc. IEEE APEC*, Anaheim, CA, Mar. 4–8, 2001, vol. 2, pp. 1123–1129.
[19] N. Celanovic and D. Boroyevich, "A fast space-vector modulation algorithm for multilevel three-phase converters," *IEEE Trans. Ind. Appl.*, vol. 37, no. 2, pp. 637–641, Mar./Apr. 2001.
[20] B. P. McGrath, T. A. Meynard, and G. Gateau, "Optimal modulation of flying capacitor and stacked multicell converters using a state machine decoder," in *Proc. IEEE PESC*, Jun. 12–16, 2005, pp. 1611–1677.
[21] R. Kennel and A. Linder, "Model predictive control for electrical drives," in *Proc. IEEE PESC*, Recife, Brazil, Jun. 2005, CD-ROM.

Pablo Correa (S'05) received the Eng. and the M.Sc. degrees in electrical engineering from the Universidad Técnica Federico Santa María, Valparaíso, Chile, in 2001. He is currently working toward the Dr.-Ing. degree at Siegen University, Siegen, Germany.

His research interests include modern control strategies for multilevel inverters.

Mario Pacas (M'96–SM'00) received the Dipl.-Ing. and Dr.-Ing. degrees in electrical engineering from the University of Karlsruhe, Karlsruhe, Germany, in 1978 and 1985, respectively.

From 1985 to 1995, he was with BBC/ABB in Switzerland and Germany in different R&D and management positions with a very wide experience in international projects. In the last years with ABB, he was responsible for the development of servo drives and later Product Responsible Manager for these products. Since 1996, he has been a member of the Faculty of Electrical Engineering and Computer Sciences, Siegen University, Siegen, Germany, and heads the Institute of Power Electronics and Electrical Drives. His special fields of interest are motion control, diagnostics, system identification, and optimization of mechatronic systems.

José Rodríguez (M'81–SM'94) received the Eng. degree in electrical engineering from the Universidad Técnica Federico Santa María, Valparaíso, Chile, in 1977, and the Dr.-Ing. degree in electrical engineering from the University of Erlangen, Erlangen, Germany, in 1985.

Since 1977, he has been with the Universidad Técnica Federico Santa María, where he is currently a Professor and a Rector. During his sabbatical leave in 1996, he was responsible for the mining division of Siemens Corporation, Chile. He has vast consulting experience in the mining industry, especially in the application of large drives like cycloconverter-fed synchronous motors for SAG mills, high-power conveyors, controlled drives for shovels, and power quality issues. His research interests are mainly in the area of power electronics and electrical drives. In recent years, his main research interests are in multilevel inverters and new converter topologies. He has authored or coauthored more than 130 refereed journal and conference papers and contributed to one chapter in the *Power Electronics Handbook* (Academic, 2001).